INVESTIGATION OF LARGE-SCALE STRUCTURES IN WALL TURBULENCE

I. Marusic, B. Ganapathisubramani, E.K. Longmire, A.K.M. Uddin*

Aerospace Engineering and Mechanics
University of Minnesota
Minneapolis, MN 55455, USA
marusic@aem.umn.edu

ABSTRACT

In this paper an experimental and theoretical investigation is presented on the role of large-scale coherent structures in the zero-pressure-gradient turbulent boundary layer. Attention is given to the proposal by Adrian, Meinhart & Tomkins (2000) that hairpin vortices are organized into spatially correlated packets or trains of vortices which extend over many boundary layer thicknesses in the streamwise direction. Support for this scenario is given here from calculations using the attached eddy model of wall turbulence of Perry & Marusic (1995). Comparisons between calculation and experiment of structure angles and two-point velocity correlations indicate that spatially coherent packets are important at least in the region of the layer where the logarithmic law of the wall applies. Preliminary experimental results are also shown of stereo-PIV measurements in the spanwise-streamwise plane of a turbulent boundary layer.

INTRODUCTION

Recent experimental and computational studies by Adrian *et al.* (2000) and Zhou *et al.* (1999) have proposed that a dominant structure in wall turbulence is the organization of hairpin vortices in spatially correlated packets or trains of vortices. This is significant since these motions are likely to be the main structure associated with near-wall transport processes. Zhou *et al.* (1999) used direct numerical simulation (DNS) to monitor the evolution of a single hairpin vortex structure embedded into the mean flow field of a low Reynolds number ($Re_\tau = 180$) turbulent channel flow. Here $Re_\tau = \delta_c U_\tau/\nu$ is the Karman number where δ_c is either boundary layer thickness or channel half-width, U_τ is wall-shear

velocity and ν is kinematic viscosity. Zhou *et al.* found that, provided the initial vortex had sufficiently high circulation in its core, then it would spawn other hairpin vortices which would consequently propagate together as a coherent packet of structures.

Adrian *et al.* (2000) experimentally studied a zero-pressure-gradient boundary layer over a Reynolds number range of $355 < Re_\tau < 2000$ using high resolution PIV (particle image velocimetry) in the wall-normal–streamwise ($x - z$) plane. Here z indicates the wall-normal direction. They concluded that the packets appear regularly in the near-wall region and in the logarithmic region of the flow extending upwards to the middle of the boundary layer. Packets containing up to 10 hairpin vortices were reported, spanning streamwise lengths up to $2\delta_c$. For this study the experimental field-of-view was restricted to $3\delta_c$. Qualitatively, the form of the packets was similar to that observed in the channel flow simulations. Adrian *et al.* showed that the idea of organized packets can explain many observations obtained from single point time-series measurements. This includes the sequence of multiple ejections associated with a burst event (Tardu 1995, Bogard & Tiederman 1986), and also the long streamwise tail in the near-wall velocity autocorrelation function known to exist since Townsend's studies in the 1950's.

In this paper, the role of packets is further studied in two ways. First, the attached eddy model of Perry & Marusic (1995) is employed to investigate whether or not packets of vortices are significant contributors to statistical quantities such as structure angles and two-point velocity correlations. Comparisons are made with corresponding experimental measurements made with hot-wire anemometry. Full details of this part of the study are given in Marusic (2001). The second part of the pa-

---

*Permanent address: Department of Mechanical Engineering, BUET, Dhaka 1000, Bangladesh.

per, presents preliminary results from a stereo-scopic PIV study in the streamwise-spanwise $(x - y)$ plane of a zero-pressure-gradient turbulent boundary layer at $Re_\tau = 1060$. While further spatial domains need to be considered, the existing results seem to support the scenario of spatially coherent regions of vortices.

VELOCITY CORRELATIONS AND STRUCTURE ANGLE

The scenario of vortex packets is first theoretically investigated using the attached eddy model of Perry & Marusic (1995). Perry & Marusic (1995) and Marusic & Perry (1995) showed how this physical model can be used to compute second order statistics, including kinetic energy spectra. Good quantitative agreement was shown for components of the Reynolds stress tensor given the experimental mean velocity flow field for a range of pressure gradients. The model, based on Townsend's (1976) attached eddy hypothesis, considers an assemblage of eddies with a range of length scales. The eddies are attached in the sense that their characteristic lengths are proportional to the distance at which the eddy is located from, or extends above, the wall. The essential feature of the attached eddy model is that it attempts to describe the kinematics of a turbulent boundary layer beyond the viscous-buffer zone, by considering a statistical ensemble of coherent vortex structures. Many length scales are considered, with the range of length scales increasing with increasing Reynolds number. Quantities of interest, such as spectra, are calculated first for a random distribution of one scale of structure (be that an individual eddy or a packet of eddies). From this, an integration across all length scales is considered with weighting functions used to account for variations in velocity scale and population density across the length scales.

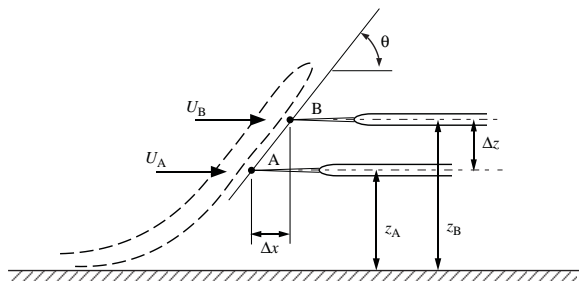In the current study, this physically based

Figure 1: Hot-wire probe arrangement and definitions. Figure from Marusic (2001).
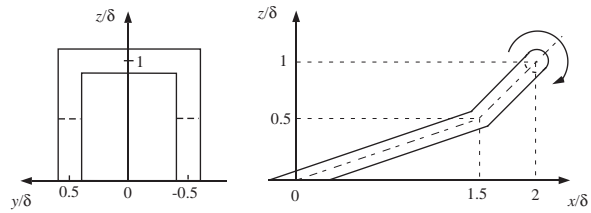

Figure 2: Details of representative attached eddy used. A Gaussian distribution of vorticity is assumed in the cores.
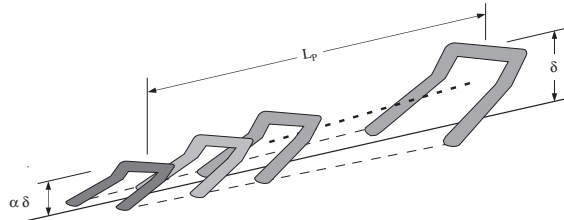

Figure 3: Schematic of packet of slanted Π-eddies.

model is used to calculate structure angles and two-point velocity correlations. Figure 1 shows the definition of terms for the two-point velocity correlation and also the experimental arrangement for which comparisons are made. The structure angle is defined as

$$\theta_i = \arctan\left(\frac{\Delta z/\delta_c}{\xi_m}\right),$$

where ξ_m is the value of $\xi = \Delta x/\delta_c$ corresponding to maximum two-point velocity correlation R_{AB} (Smits & Dussauge 1996).

Figure 2 shows the shape of eddy that was chosen for the calculations presented here. Two types of representative coherent structures are being considered. The first being individual hairpin-type structures of length scale δ, and the second being a spatially coherent packet of vortices, shown schematically in figure 3. In this case, δ is the length scale of the largest hairpin vortex in the packet. The velocity field is calculated using the Biot-Savart integral, and a Gaussian distribution of vorticity is assumed in the cores of the vortices. This part of the procedure is the same as used by Perry & Marusic (1995) and full details can be found in Marusic (2001). The procedure involves computing the representative cross-power spectrum for velocities in the z_A/δ and z_B/δ planes for one scale of eddies or packets (δ) which are randomly distributed in the $(x, y, 0)$ plane. The total cross-power spectral density comes from integrating over the range of scales, from δ_1, the smallest eddy length scale (assumed to be $100\nu/U_\tau$, the Kline et al. scaling) to δ_c, the boundary layer thickness. Weighting functions are applied for varying length scales to account for population density

and velocity scale variations between different length scales of eddies. These weighting functions are derived given the mean velocity field. Finally, the two-point correlation function is the inverse Fourier transform of this cross-power spectral density function, and normalizing this gives the two-point velocity correlation coefficient R_{AB}.

Attached eddy results

Figure 4 shows the two-point velocity correlation data for various levels throughout the boundary layer compared to experimental data of Uddin (1994). The experiment was conducted in a zero-pressure-gradient turbulent boundary layer at $Re_\tau = 4704$ ($R_\theta = 11928$). Calculations were done for both uncorrelated individual eddies and packets of the same eddy. Figure 5 shows the corresponding structure angle results. The calculations using uncorrelated eddies are seen to give poor results near the wall but good agreement in the outer part of the layer, say beyond approximately $z_A/\delta_c > 0.3$. This nominally corresponds to the region of the flow above where the logarithmic law of the wall applies. For the packet results, a simple two part calculation is used. That is, since uncorrelated eddies seem to work satisfactorily for $z_A/\delta_c > 0.3$, then only packets of spatially correlated eddies are used for approximately $\delta < 0.35\delta_c$. While this approach is crude, it is the simplest scenario possible and is shown to considerably improve the agreement with experiment. This scenario implies that the spatial cohesion of the packets breaks down for eddies $\delta > 0.35\delta_c$.

The packet chosen for these results contained 10 individual eddies, and the spatial location of each eddy in the packet was jittered, following a normal distribution, about centers corresponding to equally spaced locations between the 10 eddies. All lengths of the remaining 9 eddies were scaled geometrically (constant multiplication factor) such that the smallest eddy was height 0.2δ where δ is the height of the largest eddy in the packet. Therefore, following the notation in figure 3, $\alpha = 0.2$ and the length between the smallest and largest eddy in the packet was $L_p = 18\delta$. Since the largest packet scale was with $\delta = 0.35\delta_c$, its total length corresponds to $6.7\delta_c$.

Various combinations of L_p, number of eddies and the extent of jitter were tried. No strict importance should be attached to $L_p = 18\delta$ and $N = 10$. Other combinations were found to give comparable but slightly inferior
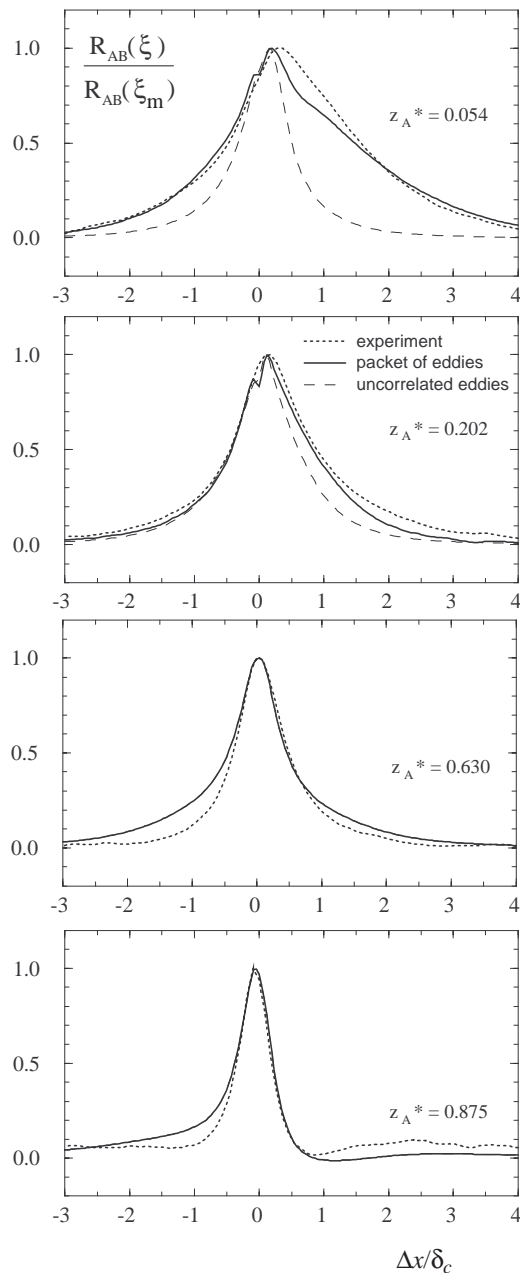

Figure 4: Normalized two-point velocity correlations at different levels through boundary layer ($z_A^* = z_A\delta_c$). For all results: $\Delta z/\delta_c = 0.096$. Dotted lines = Experimental data of Uddin (1994), $Re_\tau = 4704$. Dashed lines = Attached eddy calculation using eddies which are spatially uncorrelated (no packets). Solid line = Attached eddy calculation using packets of eddies for $\delta < 0.35\delta_c$.

agreement with the experiments. However, the important feature to note is the organization of the eddies into a packet. Many other eddy shapes and organizations of eddies were tried but only the above organization of structures into a packet was found to work. It was clear from the study that single hairpin structures that are statistically uncorrelated with any other structures could not explain the velocity correlation trends in the logarithmic region of the flow.
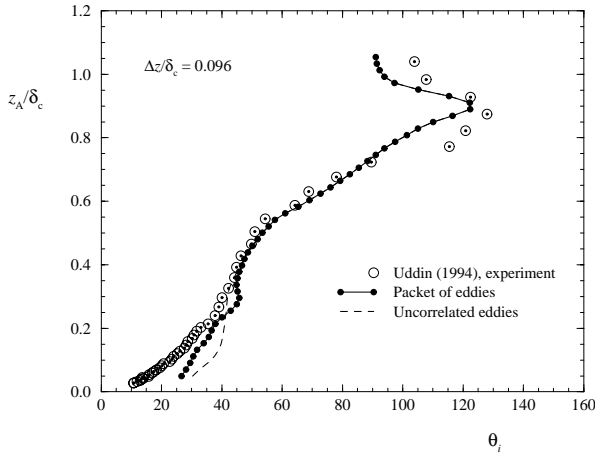
Figure 5: Structure angle results from attached eddy model compared to experiment.

PIV EXPERIMENTS

The above attached eddy calculations are based on statistically representative vortices and packets of vortices. Being statistically representative means that they have averaged features and may not necessarily be observed in any single realization. In this section, we describe the results of a stereo PIV study in streamwise-spanwise $(x - y)$ planes of a turbulent boundary layer where instantaneous features are considered. These measurements, which complement the $(x - z)$ plane data of Adrian *et al.* (2000), also yield all three components of velocity in the plane. With this information we hope to better understand the three-dimensional nature and distribution of vortices within packets and how they directly contribute to the instantaneous Reynolds shear stress and other transport properties. The results presented here show only one instant in time and one spatial domain. In future work, ensembles over many hundreds of realizations will be considered for a range of fields of view.

The measurements were carried out in a boundary layer style wind tunnel with a working section, 0.33m high, 1.22m wide and 4.8m long. The measuring station was 3.3m from the trip wire in a nominally zero-pressure-gradient flow with freestream velocity $U_1 = 5.9$ m/s. This gave a boundary layer of thickness $\delta_c = 69$ mm, with $Re_\tau = \delta_c U_\tau / \nu = 1060$ ($R_\theta = 2500$). The turbulence intensity in the freestream was less than 0.2%. Figure 6 shows the arrangement for the stereo-PIV measurements wherein the laser sheet thickness is less than 1 mm. Two Nd:YAG lasers are used to generate pulsed sheets, and images are captured by two 1024×1024 dual frame CCD cameras. Olive oil droplets (nominal size 1
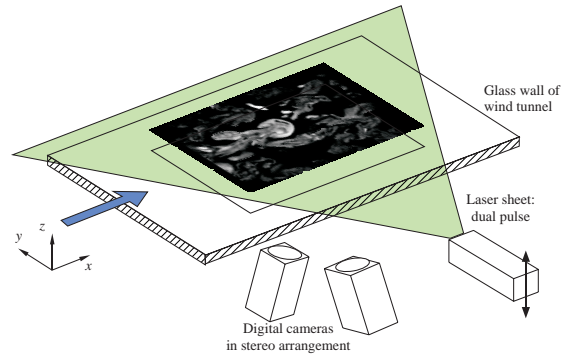

Figure 6: Stereo PIV arrangement for study.

μm), which serve as tracer particles, were feed into the intake of the wind tunnel upstream of the flow conditioning honeycomb straighteners and screens. Details of the software and stereo-calibration scheme are as given in the conference proceedings companion paper by Ganapathisubramani *et al.* (2001).

The camera field of view was set at 90 mm square. The processing of the data was for interrogation areas of 32×32 pixels with 50% overlap leaving a final velocity field just over one boundary layer thickness square. The corresponding resolution of the velocity field is therefore 2.8mm square ($0.04\delta_c$; $43\nu/U_\tau$). Therefore, for these images we have considered only relatively large scale features in the field. The measuring plane is located at $z = 6$mm ($z/\delta_c = 0.09$; $z^+ = zU_\tau/\nu = 92$) which corresponds to a level in the boundary layer where the logarithmic law of the wall applies.

Some representative results for one frame are shown in figures 7 - 10. In these figures, flow is from bottom to top. Figure 7 shows the 2D velocity field in a Galilean decomposition (Adrian, Christensen & Liu 2000) where a convection velocity of $0.6U_1$ has been subtracted from the streamwise velocity component. Figures 8, 9 and 10 show the same instantaneous field with the mean streamwise velocity ($U_{mean} = 0.65U_1$) subtracted. Superimposed are contours of instantaneous wall-normal velocity, "swirl component" S_z, and the instantaneous kinematic Reynolds shear stress $u'w'$, respectively. Following Zhou *et al.* (1999), swirl strength is defined as the imaginary part of the complex eigenvalue pair of the velocity gradient tensor, and S_z is only the part of the swirl strength derivable for $(x - y)$ plane velocity gradients. Therefore it should indicate foci-type topologies in this plane but not necessarily in the other planes. S_z is Galilean invariant and therefore is independent of the subtracted convection velocity.

The PIV data, just for this one frame, is

seen to contain a great deal of information and it is not possible to interpret the statistically important features without considering many frames and fields of view. This will be done thoroughly in on-going work. However, some notable re-occurring features have been labeled on the figures from our observations of other frames not shown because of space constrains. Figure 9 shows two fields labeled A and B that indicate typical hairpin-vortex type structures bisecting the plane. Figure 10 shows that the region of up-wash between the legs of the vortices generates large instantaneous Reynolds shear stress, as is expected. Label C shows a long streamwise zone of slower streamwise velocity straddled by approximately regularly spaced swirling zones. Such a pattern is consistent with a packet as shown in figure 3. Other examples are also evident but have not been labeled. Label D in figure 8 indicates the likely presence of the head of a hairpin-type vortex with the characteristic change in wall-normal velocity on either side of the spanwise-oriented vortex. Other regularly appearing features are long streamwise regions with approximately constant streamwise velocity over most of the field of view. Plots subtracting various streamwise velocities highlight coherent flow zones convecting at velocities within the range $0.5 - 0.9U_1$. In figure 7 we see that a large region of the flow (region E) is translating at approximately a uniform velocity which is consistent with a spatially coherent region of the flow. Regions F and G indicate spatially coherent regions spanning the entire streamwise domain that are convecting at a higher velocity.

CONCLUSIONS

Calculations of statistical quantities using the attached eddy model of Perry & Marusic (1995) suggest that spatially coherent packets are significant structures in the logarithmic region of wall turbulence. A preliminary experimental investigation has also been presented. A stereo-PIV system has been successfully implemented to give velocity field measurements in the streamwise-spanwise plane of a turbulent boundary layer. The results show the regular appearance of hairpin-type vortices, possible packet formations, and large spatially coherent regions convecting at approximately constant velocity. Further work with a large number of realizations over different fields of view is in progress.

References

R. J. Adrian, K. T. Christensen & Z.-C. Liu (2000), "Analysis and interpretation of instantaneous turbulent velocity fields" *Exp. Fluids*, vol. 29, pp. 275-290.

R. J. Adrian, C. D. Meinhart, and C. D. Tomkins (2000), "Vortex organization in the outer region of the turbulent boundary layer", *J. Fluid Mech.*, vol. 422, pp. 1-53.

D. G. Bogard and W. G. Tiederman (1986), "Burst detection with single-point velocity measurements", *J. Fluid Mech.*, vol. 162, pp. 389.

B. Ganapathisubramani, A. Loyer, E. K. Longmire, and I. Marusic (2001) "Three dimensionality in the near field of a round jet", *Proc. TSFP-2*, Stockholm, Sweden.

I. Marusic (2001), "On the role of large-scale structures in wall turbulence", *Phys. Fluids*, vol. 13(3), pp. 735-743.

I. Marusic and A. E. Perry (1995) ,"A wall-wake model for the turbulence structure of boundary layers. Part 2. Further experimental support",*J. Fluid Mech.*, vol. 298, pp. 389–407.

A. E. Perry and I. Marusic (1995) ,"A wall-wake model for the turbulence structure of boundary layers. Part 1. Extension of the attached eddy hypothesis", *J. Fluid Mech.*, vol. 298, pp. 361–388.

A. J. Smits and J. P. Dussauge (1996) *Turbulent Shear Layers in Supersonic Flow*. AIP Press, Woodbury, NY, USA.

S. Tardu (1995), "Characteristics of single and clusters of bursting events in the inner layer, Part 1: Vita events", *Exp. Fluids*, vol. 20, pp. 112.

A. A. Townsend (1976) *The Structure of Turbulent Shear Flow*. Vol.2, Cambridge University Press, Cambridge.

A. K. M. Uddin (1994),"The structure of a turbulent boundary layer", Ph.D. Thesis, University of Melbourne, Melbourne, Australia.

J. Zhou, R. J. Adrian, S. Balachandar, and T. M. Kendall (1999),"Mechanism of generating coherent packets of hairpin vortices in channel flow", *J. Fluid Mech.*, vol. 387, pp. 353–396.
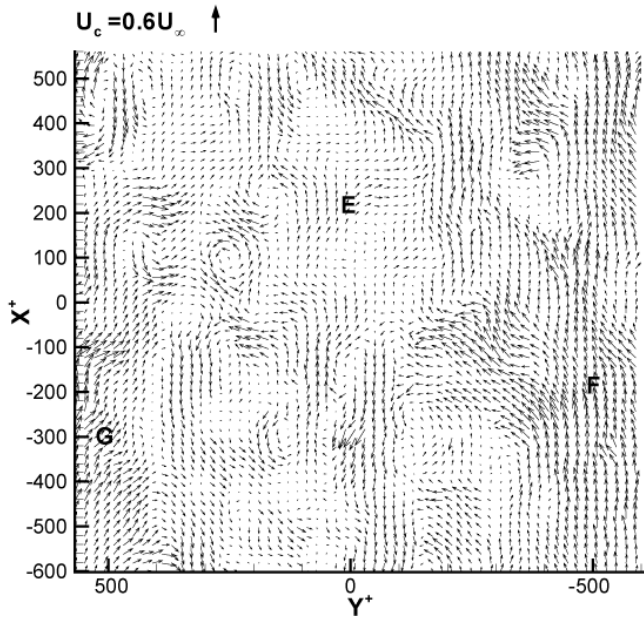
Figure 7: Streamwise-spanwise velocity field where $0.6U_1$ has been subtracted from streamwise velocity. Plane is located at $z^+ = 92$. $Re_\tau = 1060$.
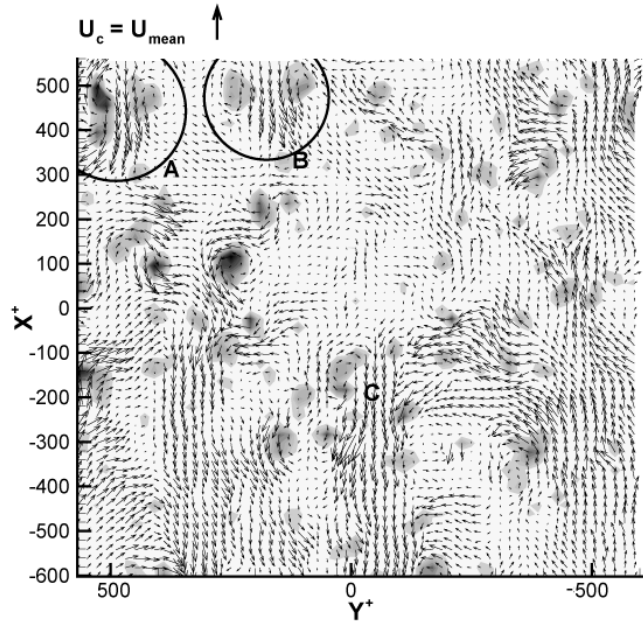

Figure 9: Velocity field same as figure 8; contours are of "swirl strength" S_z. Black and white indicate levels of 0.283 and 0.190 respectively, with gray levels distributed linearly in-between.
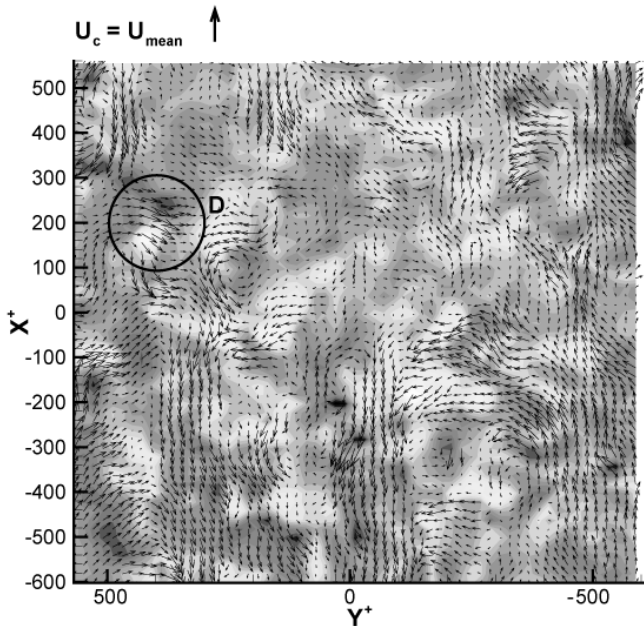

Figure 8: Streamwise-spanwise velocity field where mean velocity $(0.65U_1)$ has been subtracted from streamwise velocity. Same dataset as figure 7. Superimposed contours are of W, wall-normal velocity. Black indicates -1.30 m/s (towards wall) and white indicates 1.80 m/s (away from wall). Gray levels in-between are linearly distributed.
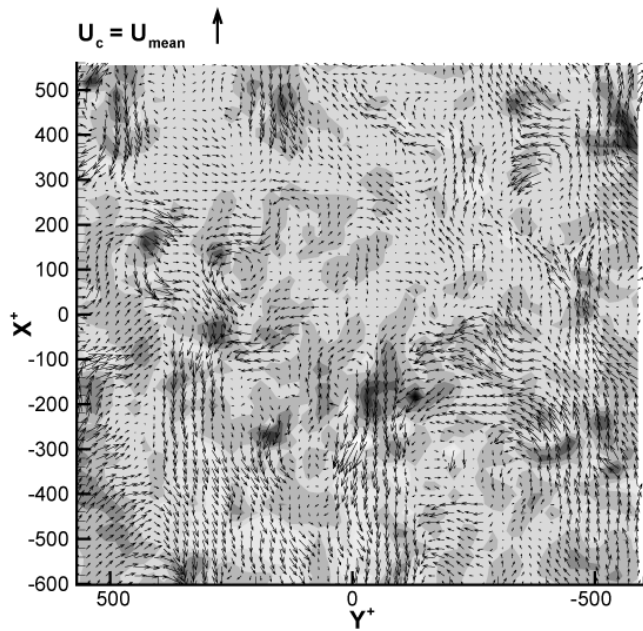

Figure 10: Velocity field same as figure 8; contours are of $u'w'/U_\tau^2$. Black and white indicate levels of -20.8 and 27.1 respectively, with gray levels distributed linearly in-between.